SF2A 2024
M. Béthermin, K. Baillié, N. Lagarde, J. Malzac, R.-M. Ouazzani, J. Richard, O. Venot, A. Siebert (eds)

CONSTRAINING SELF-INTERACTING SCALAR FIELD DARK MATTER WITH STRONG GRAVITATIONAL LENSING ?

R. Galazo-García[1], E. Jullo[1], E. Nezri[1] and M. Limousin[1]

Abstract. We present a method to constrain solitons in the Thomas-Fermi regime within the self-interacting scalar field dark matter framework. This is achieved through a semi-analytical analysis of the deflection angle in the strong gravitational lensing regime, focusing on galaxy clusters of varying masses. Specifically, we study halos with masses of $M_{200} = 2 \times 10^{15} M_\odot, 2 \times 10^{14} M_\odot$. The preliminary calculations of the deflection angle suggest that we can effectively constrain SI-SFDM particularly the soliton mass, improving our understanding of dark matter.

Keywords: Dark matter, ultra-light dark matter, scalar field dark matter, strong gravitational lensing.

1 Introduction

The Cold Dark Matter (CDM) model, which is based on Weakly Interacting Massive Particles (WIMPs), is currently the leading theory for explaining dark matter (DM) in the Universe. It is supported by strong theoretical and experimental evidence (Jungman et al. 1996; Drees et al. 2004; Steigman & Turner 1985). However, despite extensive searches, WIMPs remain undetected (Schumann 2019; Conrad 2014; Arcadi et al. 2018). Additionally, as observational techniques and numerical simulations have improved, small-scale discrepancies, known as "small-scale tensions," have emerged, challenging the CDM model(Weinberg et al. 2015; Del Popolo & Delliou 2016; Nakama et al. 2017). These tensions suggest that new physics may be needed to improve our understanding of the Universe (Di Luzio et al. 2020; Weinberg et al. 2015).

In response, alternative models like Scalar Field Dark Matter (SFDM) have been proposed (Hu et al. 2000; Hui et al. 2017; Goodman 2000). SFDM, which consists of ultra-light particles, introduces wave-like behavior on small (parsec to kiloparsec) scales. One of the most compelling features of these models is their ability to form large soliton-like structures, which can describe the core structure of galactic halos (Lee & Pang 1992; Guth et al. 2015; Sikivie & Yang 2009). These equilibrium configurations result in a smooth density profile at the center, addressing the core-cusp problem – one of the key challenges faced by CDM at galactic scales.

Detecting dark matter often involves studying its gravitational effects, such as through observations near black holes (Boudon et al. 2023) or the analysis of gravitational waves. Another promising approach is strong gravitational lensing (Sand et al. 2004; Newman et al. 2013; Limousin et al. 2022). Structures in SFDM, like solitons, could leave a gravitational imprint on the multiple images of lensed sources, offering a critical test of different dark matter models, independent of baryonic matter.

Our work specifically explores self-interacting scalar field models (SI-SFDM) (Galazo García et al. 2023) and their potential detectability using strong gravitational lensing.

2 Self-interacting scalar field dark matter dynamics

The action for the self-interacting scalar field dark matter model we consider describes a classical scalar field, ϕ, minimally coupled to gravity. It includes the standard kinetic term, with the potential $V(\phi)$ consisting of a dominant quadratic term and a secondary quartic self-interaction:

$$\mathcal{L}_\phi = -\frac{1}{2} g^{\mu\nu} \partial_\mu \phi \partial_\nu \phi - V(\phi) = -\frac{1}{2} g^{\mu\nu} \partial_\mu \phi \partial_\nu \phi - \frac{m^2}{2} \phi^2 - V_I(\phi) = -\frac{1}{2} g^{\mu\nu} \partial_\mu \phi \partial_\nu \phi - \frac{m^2}{2} \phi^2 - \frac{\lambda_4}{4} \phi^4, \quad (2.1)$$

[1] Aix–Marseille Université, CNRS, CNES, Laboratoire d'Astrophysique de Marseille, France

where m is the mass of the scalar and here λ_4 dictates the strength of the self-interactions. In the non-relativistic regime, which is relevant for astrophysical and large-scale structures, it is useful to introduce complex scalar field ψ to separate the fast oscillations at frequency m of ϕ from the slower dynamics described by ψ that follow the evolution of the density field and of the gravitational potential. Therefore, the equations of motion for the complex field ψ are given by as the Schrödinger-Poisson (SP) equations. Taking the Madelung transformation (Madelung 1926) we can rewrite the equations of motion from the field representation to the hydrodynamic framework. This allows us to describe the system in terms of a curl-free velocity field, $\vec{v}$, the density field, ρ. The dynamics are then governed by the continuity and Euler equations, along with the Poisson equation for gravity. These set of equations come from taking the real and imaginary parts of the Schrödinger equation.

$$\begin{aligned} &\partial_t \rho + \nabla \cdot (\rho \vec{v}) = 0, \\ &\partial_t \vec{v} + (\vec{v} \cdot \nabla)\vec{v} = -\nabla(\Phi_N + \Phi_I + \Phi_Q), \end{aligned} \tag{2.2}$$

with

$$\Phi_I = \frac{\rho}{\rho_a} = \rho \frac{3\lambda_4}{4m^4}, \quad \Phi_Q = -\frac{\nabla^2\sqrt{\rho}}{2m^2\sqrt{\rho}}, \tag{2.3}$$

where Φ_Q is the so-called quantum pressure. The Poisson equation for the gravitational potential reads,

$$\nabla^2 \Phi_N = 4\pi \mathcal{G}_N \rho, , \tag{2.4}$$

2.1 Solitons: Hydrostatic equilibrium and Thomas-Fermi limit

As seen from Eq.(2.2), such scalar field models admit hydrostatic equilibria given by $\vec{v} = 0$ and $\Phi_N + \Phi_I + \Phi_Q =$ constant. The spherically symmetric ground state is also called a soliton or boson star. In the Thomas-Fermi regime that we will consider in this study, this soliton is governed by the balance between gravity and the repulsive force associated with the self-interactions (for $\lambda_4 > 0$). This means that $\Phi_Q \ll \Phi_I$ over most of the extent of the soliton. Then, the hydrostatic equation that describes this state is

$$\Phi_N + \Phi_I = \frac{E}{m}. \tag{2.5}$$

An analytical solution to Eq. (2.5) can be obtained, with the soliton density profile given by Chavanis (2011); Harko (2011); Brax et al. (2019)

$$\rho_{\rm sol}(r) = \rho_{0\rm sol} \frac{\sin(\pi r/R_{\rm sol})}{\pi r/R_{\rm sol}}, \tag{2.6}$$

with the radius

$$R_{\rm sol} = \pi r_a, \ \text{ with } \ r_a^2 = \frac{3\lambda_4}{16\pi \mathcal{G}_N m^4} = \frac{1}{4\pi \mathcal{G}_N \rho_a}. \tag{2.7}$$

In fact, outside of the radius r_a where Eq.(2.6) would give a zero density we can no longer neglect Φ_Q and the exact solution develops an exponential tail at large radii.

3 Strong Gravitational lensing

The deflection angle arises from the bending of light rays as they pass near a massive object, a phenomenon predicted by General Relativity (see Bartelmann 2010, and references therein). Mass distorts spacetime, causing light to travel along a curved path. This bending effect is a fundamental aspect of gravitational lensing, where the deflection angle plays a key role in determining how light from distant objects is distorted by massive intervening objects, such as galaxies or galaxy clusters. The lens equation describes the relationship between the source position (β), the image position (θ), and the deflection angle (α). It takes into account the angular distances between the observer, the lens, and the source. Under the thin screen approximation, which assumes that the lens is much smaller than the distances involved, the lens can be treated as a two-dimensional distribution of matter. To calculate the total deflection angle, the contributions from all mass elements in the lens plane are integrated.

$$\vec{\hat{\alpha}}(\vec{\xi}) = \frac{4G}{c^2} \int \frac{(\vec{\xi} - \vec{\xi'})\Sigma(\vec{\xi'})}{|\vec{\xi} - \vec{\xi'}|^2} d^2\xi' \quad \text{with} \quad \Sigma(\vec{\xi}) = \int \rho(\vec{\xi}, z) dz. \tag{3.1}$$

The deflection angle is a two-dimensional vector, but for axially symmetric lenses that we consider in this paper, it can be calculated in just one dimension because all light rays traveling from the source to the observer must lie within the plane defined by the center of the lens, the source, and the observer. Therefore, for a symmetric mass distribution that we model, we have $\Sigma(\vec{\xi}) = \Sigma(|\vec{\xi}|)$.

4 Analytical description of dark matter halos in the self-interacting scalar field dark matter model

Fuzzy dark matter simulations reveal that the large-scale structure forms similarly to the standard CDM model (Schive et al. 2014; Veltmaat et al. 2018). These simulations generate solitonic cores within galaxies, surrounded by fluctuating halos, with the overall density profile closely matching the Navarro-Frenk-White (NFW) profile observed in the CDM model (Navarro et al. 1996). In this study, we are interested in the weak repulsive self-interactions with minimal quantum pressure at large scales. As a result, solitons are expected to form and merge within halos that undergo gravitational collapse. While the inner regions of these halos will be dominated by solitonic structures, the outer regions are still expected to follow the NFW profile. At low redshifts, the size of halos, such as galaxy clusters that we consider in this work, is much larger than r_a, making the impact of dark matter self-interactions negligible. As a result, at large radii in cosmological halos, the self-interactions have a negligible effect, and the density profile reverts to the NFW form, driven primarily by gravitational forces and dark matter velocity dispersion. Therefore, the overall density profile consists of two regions: inside the transition radius r_t, the profile is solitonic, while beyond it follows the NFW profile.

$$\begin{aligned} \rho_{\rm sol}: \quad r < r_t: \qquad & \rho(r) = \rho_{0\rm sol}\frac{\sin(\pi r/R_{\rm sol})}{\pi r/R_{\rm sol}} = \rho_{0\rm sol}\frac{\sin(r/r_a)}{r/r_a}, \\ \rho_{\rm NFW}: \quad r_t < r < R_{200}: \qquad & \rho(r) = \frac{\rho_s}{\frac{r}{r_s}\left(1+\frac{r}{r_s}\right)^2}. \end{aligned} \tag{4.1}$$

The transition radius is calculated as the position at which the following equality is satisfied:

$$M_{\rm sol}(r_t) = \alpha M_{\rm NFW}(r_t) \tag{4.2}$$

The α parameter in Eq.(4.2) quantifies how the soliton's mass within r_t compares to the NFW mass. In practice, we replace the NFW mass with the soliton mass at r_t, ensuring continuity and total mass conservation of the halo. However, to ensure that we do not exclude any potential configurations and to allow for greater flexibility in the soliton's mass setup, we introduce the parameter α. This approach is justified as long as we stay within the Newtonian regime and the total system mass undergoes minimal changes.

4.1 Building the self-interacting dark matter halo profiles

To define the total density profile, we need to establish parameters for the NFW component, specifically ρ_s and r_s, along with the transition radius r_t, and parameters for the solitonic component $\rho_{0\rm sol}$ and r_a.

We start by determining the NFW profile, which involves calculating ρ_s and r_s. First, we select the mass M_{200} and redshift z_l of the halo that acts as the lens in our gravitational lensing analysis. Following that, we compute $R_{200} = \left(\frac{3M_{200}}{4\pi 200\rho_{crit}(z_l)}\right)^{1/3}$. Next, we obtain the halo concentration c from (Ishiyama et al. 2020) and use it to compute r_s based on the relation $c = \frac{R_{200}}{r_s}$. To determine ρ_s we solve the equation that ensures the integrated mass of the system at R_{200} is equal to the selected mass M_{200}: $M_{\rm NFW}(R_{200}) = M_{200}$. For the soliton profile, we first set the theoretical framework we are interested in, selecting the parameter r_a. We also set the mass factor α. We then calculate the pair of values of r_t and ρ_{0sol} that correspond to the soliton mass defined by α, thereby completing the profile. We have some flexibility in choosing α as long as we remain within the Newtonian regime and the mass of the system varies minimally.

5 Results

In Fig.1, we present the density profiles for two halos: mass 1 on the left and mass 2 on the right. We analyze various self-interacting scalar mass models with scales of 5 kpc and 15 kpc. Additionally, we examine two different values for the α factor, 1 and 3, as the total system mass varies by less than 2% in both cases. For comparison, the NFW profile is also shown in both figures. At larger radii, all configurations converge to the

NFW profile, while the central region is modified by design. This suggests that the deflection angle could account for this variation, which is why Figure 2 presents the comparison of the deflection angle difference, calculated using Eq.(3.1), between the NFW profile alone and the self-interacting scalar field dark matter profiles.

In certain configurations – for a halo mass of $M_{200} = 2 \times 10^{14} M_\odot$ with $\alpha = 3$ and $r_a = 5, 15$ kpc, as well as for $M_{200} = 2 \times 10^{15} M_\odot$ with the same α and r_a values – the deflection angle differs by more than 2 arcseconds, suggesting that these deviations could provide insights into differences in dark matter distribution when analyzing gravitational lensing data.

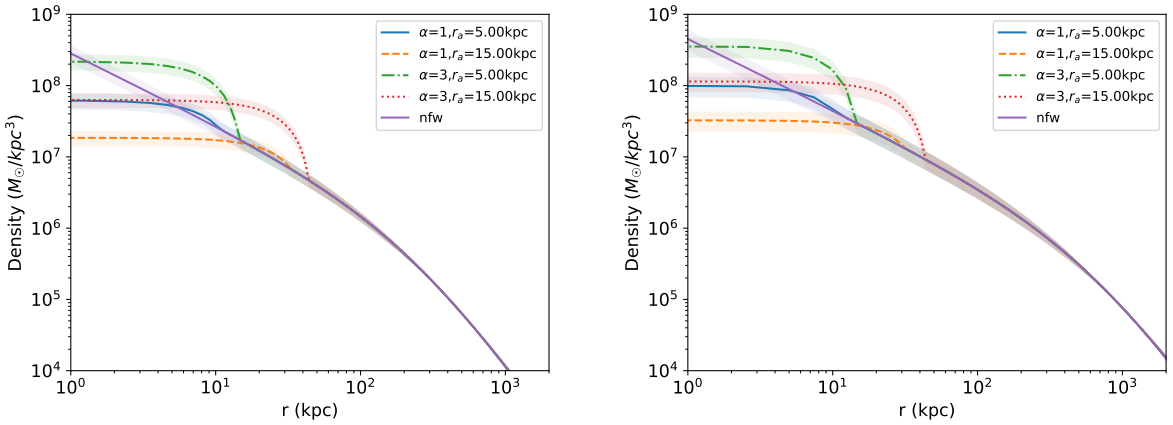

Fig. 1. Density profile for different SI-SFDM halos with mass factors $\alpha = 1$ and $\alpha = 3$ and with self-interacting scales $r_a = 5$ kpc and 15 kpc compared with the NFW profile in purple. **Left:** Halo of $M_{200} = 2 \times 10^{14} M_\odot$ **Right:** Halo of $M_{200} = 2 \times 10^{15} M_\odot$.

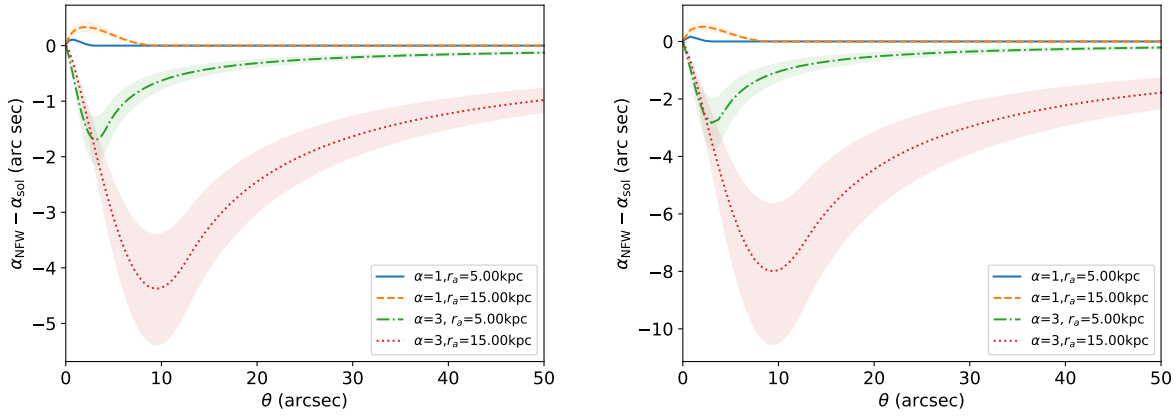

Fig. 2. Difference between the deflection angle produced by a NFW halo (CDM) and a soliton+NFW halo (SI-SFDM) for mass factors $\alpha = 1$ and $\alpha = 3$ and for self-interacting scales $r_a = 5$ kpc and 15 kpc. **Left:** Halo of $M_{200} = 2 \times 10^{14} M_\odot$ **Right:** Halo of $M_{200} = 2 \times 10^{15} M_\odot$.

6 Conclusions

The distinct gravitational lensing patterns resulting from differences between standard and SFDM density profiles offer a way to differentiate between these models. Preliminary results suggest that we can effectively constrain SI-SFDM parameters, improving our understanding of dark matter. Our findings align well with McClintock et al. (2018), particularly in the weak lensing mass calibration at large scales, confirming the validity of our approach. Additionally, comparisons with Newman et al. (2013) show a good fit, and we establish an upper limit on the soliton mass of $M_{sol} \sim 10^{12} M_\odot$ for certain configurations, contributing to a more precise SFDM model. Future strong lensing observations will be crucial for probing SFDM properties, especially in cluster centers where the effects are more prominent.

References

Arcadi, G., Dutra, M., Ghosh, P., et al. 2018, European Physical Journal C, 78, 203

Bartelmann, M. 2010, Classical and Quantum Gravity, 27, 233001

Boudon, A., Brax, P., Valageas, P., & Wong, L. K. 2023, Physical Review D, 109

Brax, P., Cembranos, J. A. R., & Valageas, P. 2019, Phys. Rev. D, 100, 023526

Chavanis, P.-H. 2011, Phys. Rev. D, 84, 043531

Conrad, J. 2014, arXiv e-prints, arXiv:1411.1925

Del Popolo, A. & Delliou, M. L. 2016, Galaxies, 5

Di Luzio, L., Giannotti, M., Nardi, E., & Visinelli, L. 2020, Physics Reports, 870, 1

Drees, M., Godbole, R., & Roy, P. 2004, Theory and phenomenology of sparticles: An account of four-dimensional N=1 supersymmetry in high energy physics

Galazo García, R., Brax, P., & Valageas, P. 2023, arXiv e-prints, arXiv:2304.10221

Goodman, J. 2000, New A, 5, 103

Guth, A. H., Hertzberg, M. P., & Prescod-Weinstein, C. 2015, Phys. Rev. D, 92, 103513

Harko, T. 2011, Mon. Not. Roy. Astron. Soc., 413, 3095

Hu, W., Barkana, R., & Gruzinov, A. 2000, Phys. Rev. Lett., 85, 1158

Hui, L., Ostriker, J. P., Tremaine, S., & Witten, E. 2017, Phys. Rev. D, 95, 043541

Ishiyama, T., Prada, F., Klypin, A. A., et al. 2020, Monthly Notices of the Royal Astronomical Society, 506, 4210

Jungman, G., Kamionkowski, M., & Griest, K. 1996, Phys. Rep., 267, 195

Lee, T. D. & Pang, Y. 1992, Phys. Rept., 221, 251

Limousin, M., Beauchesne, B., & Jullo, E. 2022, A&A, 664, A90

Madelung, E. 1926, Ann. d. Phys, 79

McClintock, T., Varga, T. N., Gruen, D., et al. 2018, Monthly Notices of the Royal Astronomical Society, 482, 1352–1378

Nakama, T., Chluba, J., & Kamionkowski, M. 2017, Physical Review D, 95, 121302

Navarro, J. F., Frenk, C. S., & White, S. D. M. 1996, Astrophys. J., 462, 563

Newman, A. B., Treu, T., Ellis, R. S., & Sand, D. J. 2013, The Astrophysical Journal, 765, 25

Sand, D. J., Treu, T., Smith, G. P., & Ellis, R. S. 2004, ApJ, 604, 88

Schive, H. Y., Chiueh, T., & Broadhurst, T. 2014, Nature Physics, 10, 496

Schumann, M. 2019, Journal of Physics G Nuclear Physics, 46, 103003

Sikivie, P. & Yang, Q. 2009, Phys. Rev. Lett., 103, 111301

Steigman, G. & Turner, M. S. 1985, Nuclear Physics B, 253, 375

Veltmaat, J., Niemeyer, J. C., & Schwabe, B. 2018, Phys. Rev. D, 98, 043509

Weinberg, D. H., Bullock, J. S., Governato, F., De Naray, R. K., & Peter, A. H. 2015, Proceedings of the National Academy of Sciences of the United States of America, 112, 12249